Electronic Supplementary Information for

A ferrocene-containing analogue of the MCU inhibitor Ru265 with increased cell permeability

Zhouyang Huang,[a] Jesse A. Spivey,[a] Samantha N. MacMillan,[a] and Justin J. Wilson*[a]

[a]Department of Chemistry and Chemical Biology, Cornell University, Ithaca, NY 14853, USA.

*Email: jjw275@cornell.edu

Table of Contents

1. General

Materials and Reagents. All reagents were purchased from commercial vendors. All solvents were of ACS grade or higher. $[Ru_2(\mu\text{-}N)(NH_3)_8(Cl)_2](Cl)_3$ (Ru265)[1] and sodium ferrocenecarboxylate ($NaFcCO_2$)[2] were synthesized as previously described. No specific precautions were taken to exclude air or water from reactions. Water (18 MΩ·cm) was purified using an ELGA PURELAB flex 2 (High Wycombe, UK).

Physical Measurements. NMR samples were prepared in DMSO-d_6. For ^{1}H and ^{19}F NMR spectroscopy, samples were analyzed on a 400 MHz Bruker AV 3HD spectrometer with BBFO broadband probe. For $^{13}C\{^1H\}$ NMR spectroscopy, samples were analyzed on a 500 MHz Bruker AV 3HD spectrometer equipped with a broadband Prodigy cryoprobe. ^{1}H NMR chemical shifts were referenced internally to the chemical shift of residual DMSO-d_5 (δ = 2.50 ppm) relative to tetramethylsilane (δ = 0 ppm). ^{19}F NMR chemical shifts were referenced to $CFCl_3$ (δ = 0 ppm) with an external standard of KPF_6 in D_2O (δ = –72 ppm). $^{13}C\{^1H\}$ NMR chemical shifts were referenced to the DMSO peak at 39.52 ppm. Infrared spectra were collected on a Bruker Tensor II IR spectrometer with a diamond attenuated total reflectance (ATR) attachment. Elemental analysis (CHN) was performed by Atlantic Microlab Inc. (Norcross, GA, USA). High-performance liquid chromatography (HPLC) was carried out on a system consisting of a CBM-20A communications bus module, an LC-20AT (analytical) pump, and an SPD-20AV UV-vis detector monitoring at 270 nm (Shimadzu, Japan). Analytical HPLC was carried out using an Ultra Aqueous C18 column, 100 Å, 5 μm, 250 mm × 4.6 mm (Restek, Bellefonte, PA) at a flow rate of 1.0 mL/min. UV-vis spectra were acquired using a Shimadzu UV-1900 spectrophotometer (Shimadzu, Kyoto, Japan) fitted with a temperature-controlled circulating water bath. Fluorescence and absorbance of samples in 96-well plates were measured using a BioTek Synergy HTX plate reader (Agilent, Santa Clara, CA). Graphite furnace atomic absorption spectroscopy (GFAAS) was performed using a PerkinElmer PinAAcle 900z spectrometer (PerkinElmer, Waltham, MA). Statistical analyses were performed using GraphPad Prism 9.2.0 software by applying non-paired student's t-tests.

2. Synthesis and Characterization

Synthesis of $[Ru_2(\mu\text{-}N)(NH_3)_8(H_2O)_2](OTf)_5$ (Ru265′). To a stirring suspension of Ru265 (315 mg, 0.6 mmol) in water (30 mL) was added AgOTf (715 mg, 2.8 mmol). This mixture was then heated at reflux in the dark for 4 h. The white precipitate AgCl was removed via vacuum filtration, and the filtrate was lyophilized to yield a pale orange powder. Yield: 640 mg (0.564 mmol, 95%). The material was used in the next step without further purification. ^{1}H NMR (400 MHz, DMSO-d_6): δ 3.97 (24H).

Synthesis of $[Ru_2(\mu\text{-}N)(NH_3)_8(PhCO_2)_2](OTf)_3$ (RuOBz). To a stirring solution of Ru265′ (80 mg, 0.07 mmol) in methanol (8 mL) was added sodium benzoate (20 mg, 0.14 mmol). The resulting mixture was heated at 50 °C for 3 h in the dark, after which the methanol was removed under reduced pressure. To the resulting orange residue, tetrahydrofuran (THF, 2 mL) was added, and the solution was filtered and then layered with hexane (4 mL). Storage of this solution at –20 °C for 24 h resulted in the deposition of products as yellow orange microcrystals, which were isolated by decanting the supernatant, washed with diethyl ether (3 × 1 mL), and dried *in vacuo*. After repeating the same layering step two more times, the orange microcrystals were dissolved in 8 mL of THF, and the resulting solution was partitioned into two vials, which were subjected to vapor diffusion of hexane for 48 h at room temperature. The resulting yellow crystals were combined to obtain 20 mg of pure product (0.019 mmol, 27%). ^{1}H NMR (400

MHz, DMSO-d_6): δ 7.94 (d, J = 6.8 Hz, 4H), 7.48 (t, J = 7.3 Hz, 2H), 7.39 (t, J = 7.6 Hz, 4H), 4.08 (s, 24H). $^{13}C\{^1H\}$ NMR (126 MHz, DMSO-d_6): δ 173.26, 135.70, 131.04, 129.42, 127.57, 124.52, 121.95, 119.39, 116.82. ^{19}F NMR (376 MHz, DMSO-d_6): δ –77.74. IR (ATR, cm^{-1}): 1600 m, 1566 m, 1026 s. Anal. Calcd for $[C_{14}H_{34}N_9O_4Ru_2](OTf)_3$: C, 19.60; H, 3.29; N, 12.10. Found: C, 19.84; H, 3.33; N, 11.71.

Synthesis of $[Ru_2(\mu\text{-}N)(NH_3)_8(FcCO_2)_2](OTf)_3$ (RuOFc). To a stirring solution of Ru265′ (80 mg, 0.07 mmol) in methanol (8 mL), was added sodium ferrocenecarboxylate (35 mg, 0.14 mmol). The resulting mixture was heated at 50 °C for 3 h in the dark. The methanol was removed under reduced pressure. To the resulting orange oil, THF (2 mL) was added, and the solution was filtered and then layered with diethyl ether (5 mL). Storage of this solution at –20 °C for 24 h resulted in the deposition of products as red crystals, which were isolated by decanting the supernatant. These crystals were quickly washed first with isopropanol (3 × 1 mL) and then with diethyl ether (3 × 1 mL), and dried *in vacuo*. Yield: 41 mg (0.033 mmol, 47%). ^1H NMR (400 MHz, DMSO-d_6): δ 4.62 (t, J = 1.9 Hz, 4H), 4.28 (t, J = 2.0 Hz, 4H), 4.17 (s, 10H), 4.03 (s, 24H). $^{13}C\{^1H\}$ NMR (126 MHz, DMSO-d_6): δ 178.16, 124.52, 121.95, 119.38, 116.82, 77.52, 69.96, 69.61, 69.14. ^{19}F NMR (376 MHz, DMSO-d_6): δ –77.74. IR (ATR, cm^{-1}): 1606 m, 1528 m, 1023 s. Anal. Calcd for $[C_{22}H_{42}Fe_2N_9O_4Ru_2](OTf)_3$: C, 23.88; H, 3.37; N, 10.02. Found: C, 23.71; H, 3.27; N, 9.79.

X-ray Crystallography. Suitable crystals of **RuOBz** were grown from the diffusion of diethyl ether into a DMF solution of the nitrate salt of **RuOBz**, which was stored at room temperature for several days. Suitable crystals of **RuOFc** were grown from the diffusion of diethyl ether (5 mL) into a THF solution of **RuOFc** (5 mg in 1 mL), which was stored at room temperature for 48 h. Low-temperature X-ray diffraction data for **RuOBz** and **RuOFc** were collected on a Rigaku XtaLAB Synergy diffractometer coupled to a Rigaku Hypix detector with Cu Kα radiation (λ = 1.54184 Å), from a PhotonJet micro-focus X-ray source at 100 K. The diffraction images were processed and scaled using the CrysAlisPro software (Rigaku Oxford Diffraction, The Woodlands TX, 2015). The structures were solved through intrinsic phasing using SHELXT[3] and refined against F^2 on all data by full-matrix least squares with SHELXL[4] following established refinement strategies.[5] All non-hydrogen atoms were refined anisotropically. All hydrogen atoms bound to carbon were included in the model at geometrically calculated positions and refined using a riding model. The isotropic displacement parameters of all hydrogen atoms were fixed to 1.2 times the Ueq value of the atoms they are linked to (1.5 times for methyl groups). In the structure of **RuOFc**, an electron density peak was assigned to be a disordered water molecule (O4S). Its occupancy was refined to a value of 0.25, which gave acceptable displacement parameters for the water O atom. **RuOBz** contains disordered solvent molecules of MeOH that were included in the unit cell but could not be satisfactorily modeled. Therefore, those solvents were treated as diffuse contributions to the overall scattering without specific atom positions using the solvent mask routine in Olex2.[6] The program has identified a void of 30 $Å^3$ with 27 electrons, which is consistent with the presence of 1.5 MeOH. Details of the data quality and a summary of the residual values of the refinements are listed in **Table S1**. CCDC 2212058-2212059 contain the supplementary crystallographic data for this paper. These data can be obtained free of charge via www.ccdc.cam.ac.uk/data_request/cif, or by emailing data_request@ccdc.cam.ac.uk, or by contacting The Cambridge Crystallographic Data Centre, 12 Union Road, Cambridge CB2 1EZ, UK; fax: +44 1223 336033.

Table S1. X-ray crystal data and structure refinement details for **RuOBz** and **RuOFc**.

Compound	**RuOBz**	**RuOFc**
Empirical Formula	$C_{21.50}H_{54}N_{13}O_{13.50}Ru_2$	$C_{33}H_{60.50}F_9Fe_2N_9O_{16.25}Ru_2S_3$
Formula Weight	912.91	1424.42
a (Å)	8.9493(2)	11.46050(10)
b (Å)	9.6266(2)	31.7571(2)
c (Å)	12.3811(3)	15.37260(10)
α (°)	74.463(2)	90
β (°)	77.682(2)	108.7930(10)
γ (°)	63.195(2)	90
V (Å^3)	911.92(4)	5296.62(7)
Z	1	4
Crystal System	Triclinic	Monoclinic
Space Group	$P\bar{1}$	$P2_1/c$
ρ_{calc} (Mg/m^3)	1.662	1.786
μ (mm^{-1})	7.382	10.867
T (K)	100.01(10)	99.9(7)
θ range (°)	3.727 to 70.064	2.783 to 78.124
Independent Reflections	3459	11241
R_{int}	0.0579	0.0518
Number of Parameters	268	773
Largest diff. peak and hole (e·Å^{-3})	1.106/-0.926	1.300/-1.040
GoF	1.068	1.036
R1/wR2 (all data)	0.0357/0.0899	0.0380/0.0905
R1/wR2 (I >2σ)	0.0340/0.0885	0.0352/0.0888

$R_1 = \Sigma||F_o|-|F_c||/\Sigma|F_o|$; $wR2 = \{\Sigma[w(F_o^2-F_c^2)^2]/\Sigma([F_o^2)^2]\}^{1/2}$

GoF = $\{\Sigma[w(F_o^2-F_c^2)^2]/(n-p)\}^{1/2}$, where *n* is the number of data and *p* is the number of refined parameters.

Table S2. Selected interatomic distances and angles for **RuOBz** and **RuOFc**.

Distances (Å) for **RuOBz**		Distances (Å) for **RuOFc**			
Ru–O(1)	2.099(2)	Ru(1)–O(1)	2.104(2)	Ru(2)–O(3)	2.091(2)
Ru–N(1)	1.7394	Ru(1)–N(1)	1.740(3)	Ru(2)–N(1)	1.740(3)
Ru–N(2A)	2.17(1)	Ru(1)–N(2)	2.114(3)	Ru(2)–N(6)	2.116(2)
Ru–N(3)	2.099(5)	Ru(1)–N(3)	2.106(2)	Ru(2)–N(7)	2.119(2)
Ru–N(4)	2.112(2)	Ru(1)–N(4)	2.130(3)	Ru(2)–N(8)	2.116(2)
Ru–N(5)	2.113(5)	Ru(1)–N(5)	2.127(2)	Ru(2)–N(9)	2.098(2)
Angles (°) for **RuOBz**		Angles (°) for **RuOFc**			
O(1)–Ru–N(1)	178.4	O(1)–Ru(1)–N(1)	178.5(1)	O(3)–Ru(2)–N(1)	177.0(1)
O(1)–Ru–N(2A)	83.3(3)	O(1)–Ru(1)–N(2)	87.39(9)	O(3)–Ru(2)–N(6)	85.89(9)
O(1)–Ru–N(3)	87.5(1)	O(1)–Ru(1)–N(3)	87.36(9)	O(3)–Ru(2)–N(7)	91.70(9)
O(1)–Ru–N(4)	88.5(1)	O(1)–Ru(1)–N(4)	86.36(9)	O(3)–Ru(2)–N(8)	84.00(9)
O(1)–Ru–N(5)	82.9(1)	O(1)–Ru(1)–N(5)	83.06(9)	O(3)–Ru(2)–N(9)	81.42(9)
N(1)-Ru–N(2A)	95.8	N(1)-Ru(1)–N(2)	91.9(1)	N(1)-Ru(2)–N(6)	94.4(1)
N(1)–Ru–N(3)	93.6	N(1)–Ru(1)–N(3)	93.9(1)	N(1)–Ru(2)–N(7)	91.3(1)
N(1)–Ru–N(4)	92.57	N(1)–Ru(1)–N(4)	94.3(1)	N(1)–Ru(2)–N(8)	95.7(1)
N(1)–Ru–N(5)	95.9	N(1)–Ru(1)–N(5)	95.6(1)	N(1)–Ru(2)–N(9)	95.6(1)
N(2A)–Ru–N(3)	80.7(3)	N(2)–Ru(1)–N(3)	89.25(9)	N(6)–Ru(2)–N(7)	90.05(9)
N(2A)–Ru–N(4)	167.3(3)	N(2)–Ru(1)–N(4)	173.8(1)	N(6)–Ru(2)–N(8)	169.9(1)
N(2A)–Ru–N(5)	98.8(3)	N(2)–Ru(1)–N(5)	90.28(9)	N(6)–Ru(2)–N(9)	89.74(9)
N(3)–Ru–N(4)	89.3(1)	N(3)–Ru(1)–N(4)	90.47(9)	N(7)–Ru(2)–N(8)	90.82(9)
N(3)–Ru–N(5)	170.4(2)	N(3)–Ru(1)–N(5)	170.4(1)	N(7)–Ru(2)–N(9)	173.12(9)
N(4)–Ru–N(5)	89.7(1)	N(4)–Ru(1)–N(5)	88.96(9)	N(8)–Ru(2)–N(9)	88.20(9)

Atoms are labelled as shown in **Fig. 1**. Values in parentheses indicate the standard uncertainty in the last significant figure.

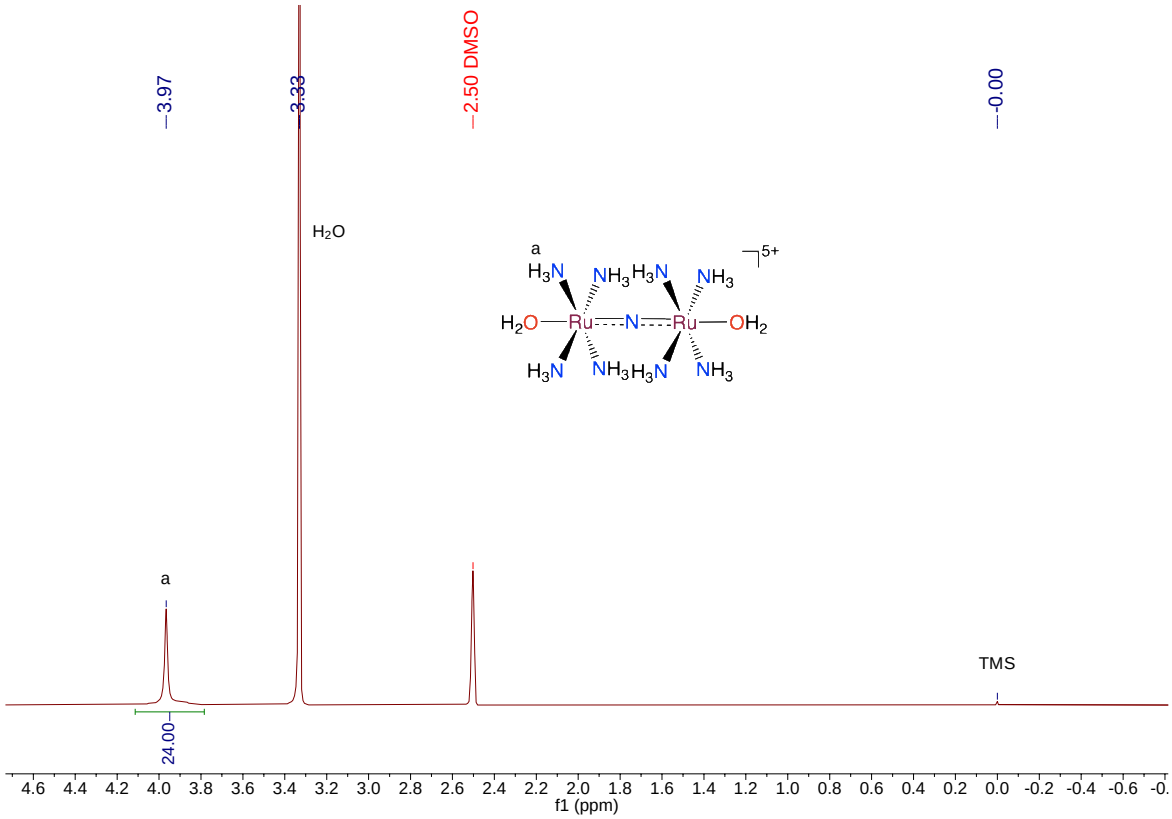

Fig. S1 ^{1}H NMR spectrum of Ru265′ in DMSO-d_6 (400 MHz, 25 °C).

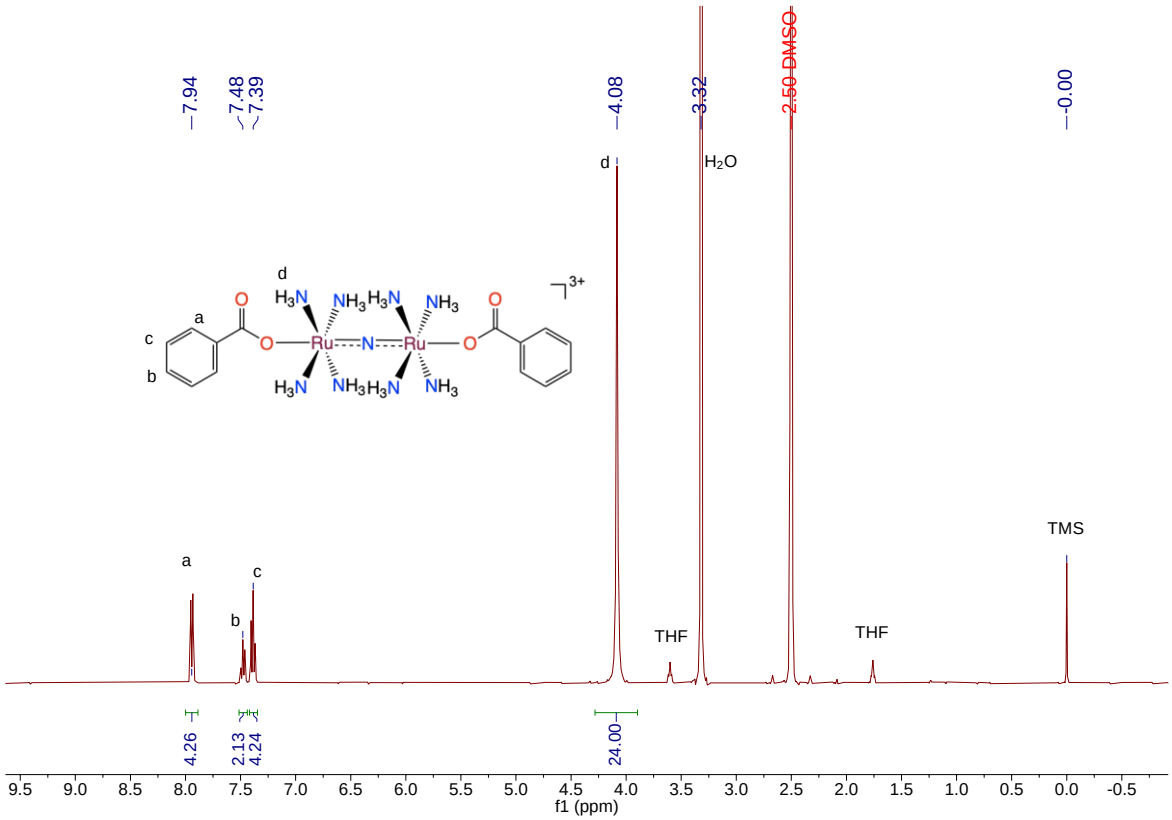

Fig. S2 ^{1}H NMR spectrum of **RuOBz** in DMSO-d_6 (400 MHz, 25 °C).

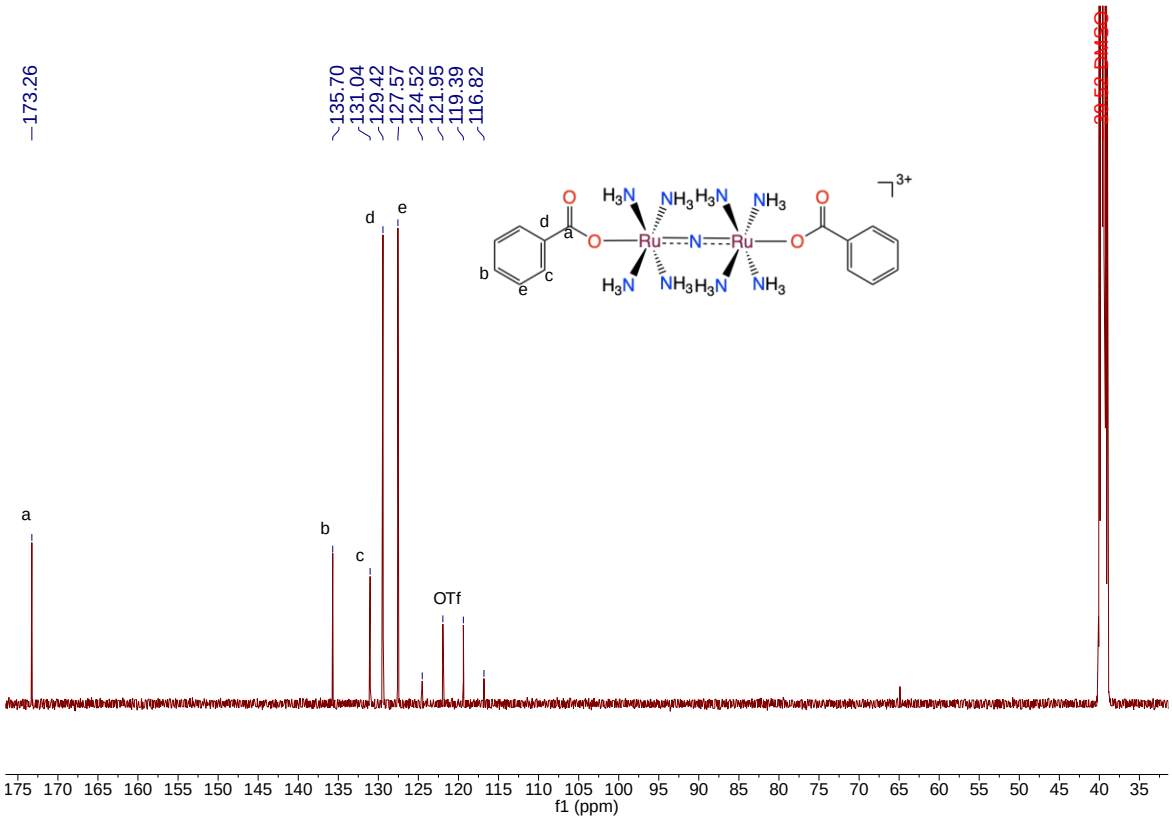

Fig. S3 ^{13}C{^{1}H} NMR spectrum of **RuOBz** in DMSO-d_6 (126 MHz, 25 °C).

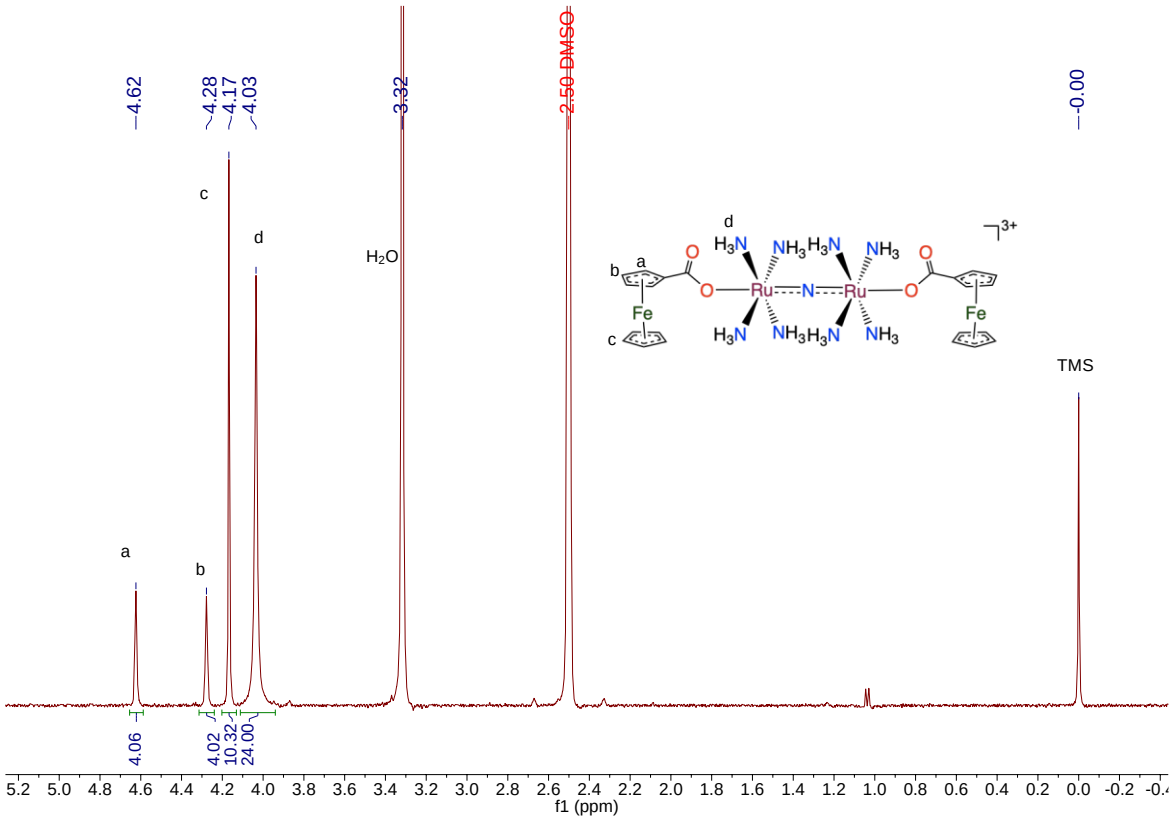

Fig. S4 ^{1}H NMR spectrum of **RuOFc** in DMSO-d_6 (400 MHz, 25 °C).

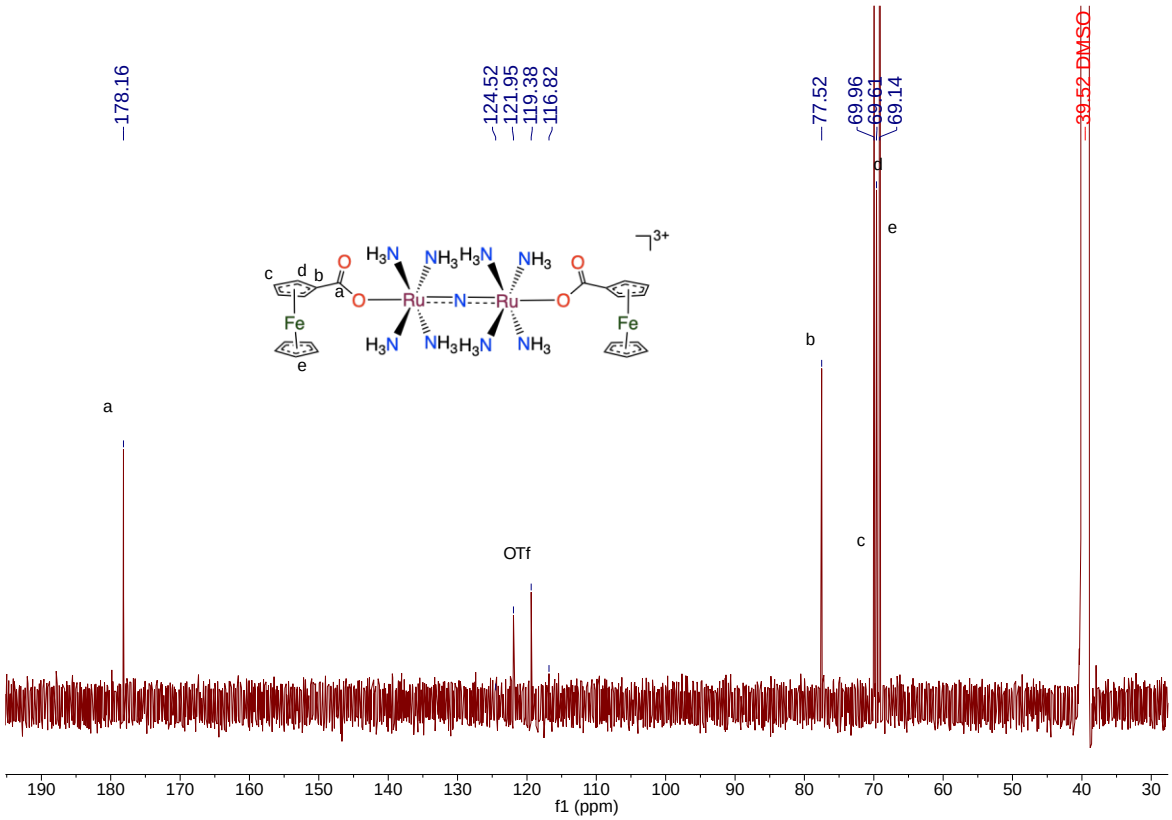

Fig. S5 ^{13}C{^{1}H} NMR spectrum of **RuOFc** in DMSO-d_6 (126 MHz, 25 °C).

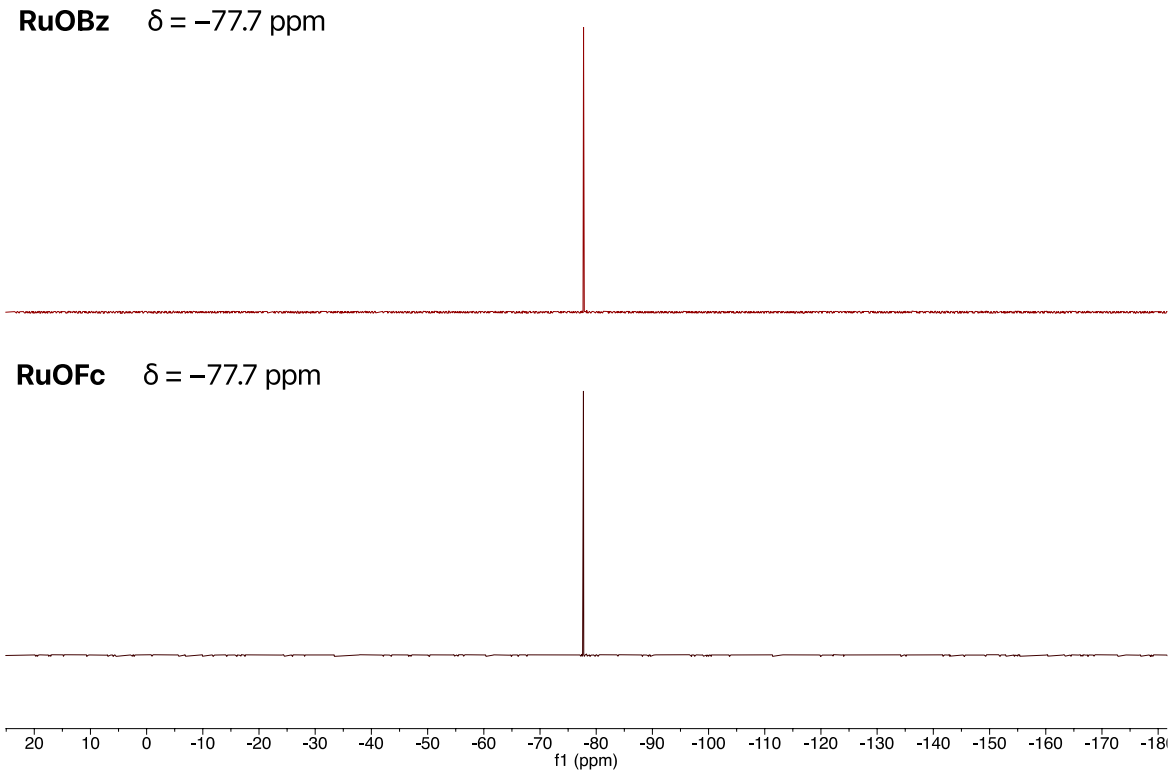

Fig. S6 ^{19}F NMR spectrum of **RuOBz** and **RuOFc** in DMSO-d_6 (376 MHz, 25 °C).

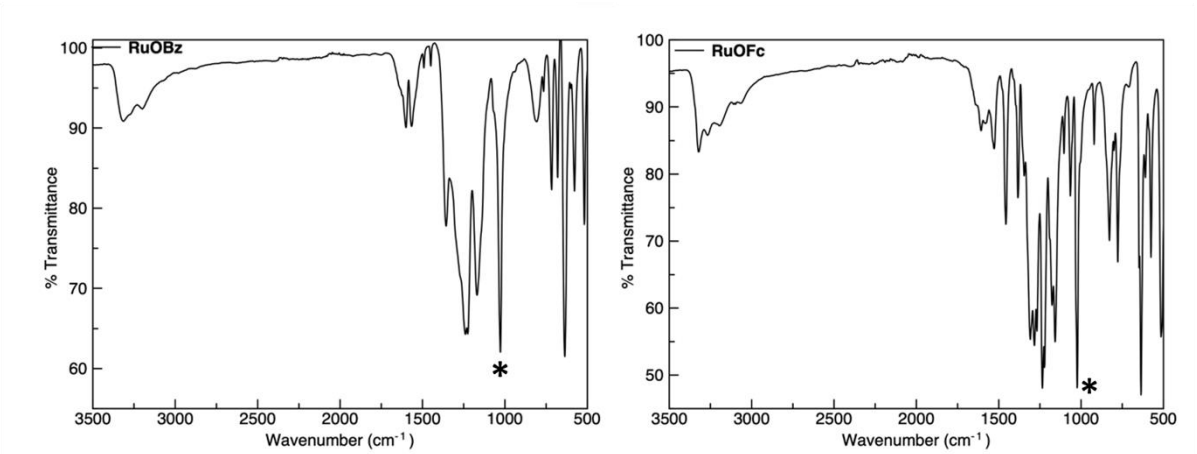

Fig. S7 IR spectra of **RuOBz** and **RuOFc**. The asterisks indicate the asymmetric Ru–N–Ru stretches.

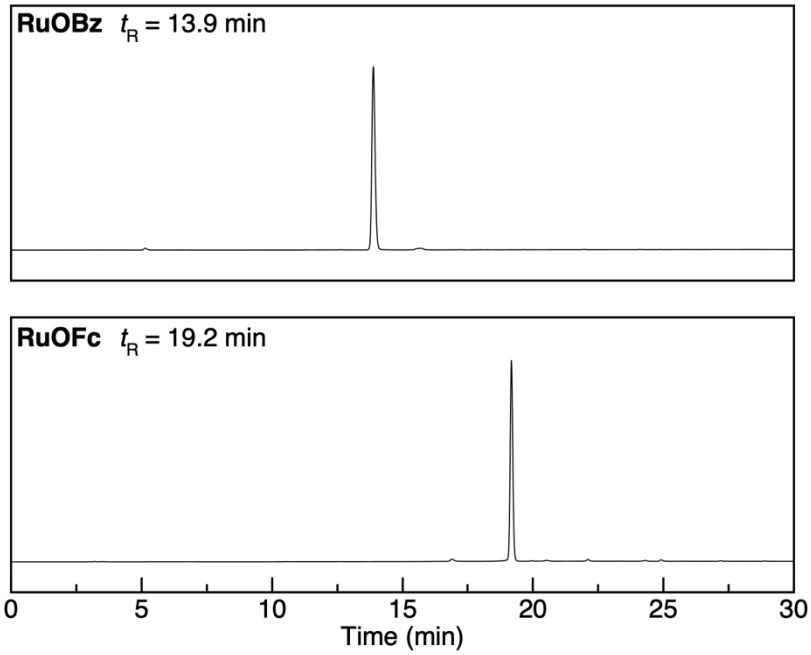

Fig. S8 HPLC chromatograms of **RuOBz** and **RuOFc**. Gradient: 0−5 min, 10% MeOH in H_2O; 5−25 min, 10−100% MeOH in H_2O; 25−30 min, 100% MeOH. The mobile phase contains 0.1% trifluoroacetic acid (TFA).

Lipophilicity Measurement. The logarithm values of n-octanol-water partition coefficients (log *P*) were measured using an established HPLC-based protocol.[7] An isocratic HPLC elution mode was employed with a mobile phase containing 40% MeOH in H_2O with 0.1% TFA. The dead time (t_0) of the column was determined using a solution of thiourea, which has no retention on the C18 column. The retention times (t_r) of 5 standard compounds, as well as **RuOFc** and **RuOBz**, were measured (**Fig. S9**), and their retention factors (k) were calculated ($k = (t_r – t_0)/t_0$). The literature log *P* values of the 5 standard compounds were plotted against their log *k* values to create a linear calibration curve (**Fig. S10**). All literature log *P* values are from ref 7, except for hydroquinone and catechol.[8] Using the calibration curve, the log *P* values of **RuOFc** and **RuOBz** were extrapolated from their log *k* values.

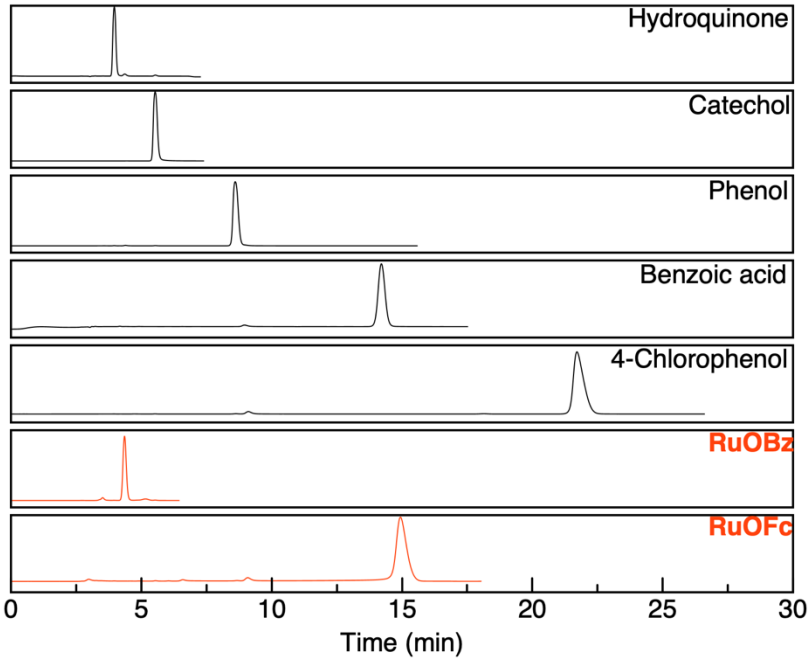

Fig. S9 HPLC chromatograms of 5 standard compounds, **RuOBz** and **RuOFc**. Isocratic elution mode: 40% MeOH in H_2O with 0.1% TFA.

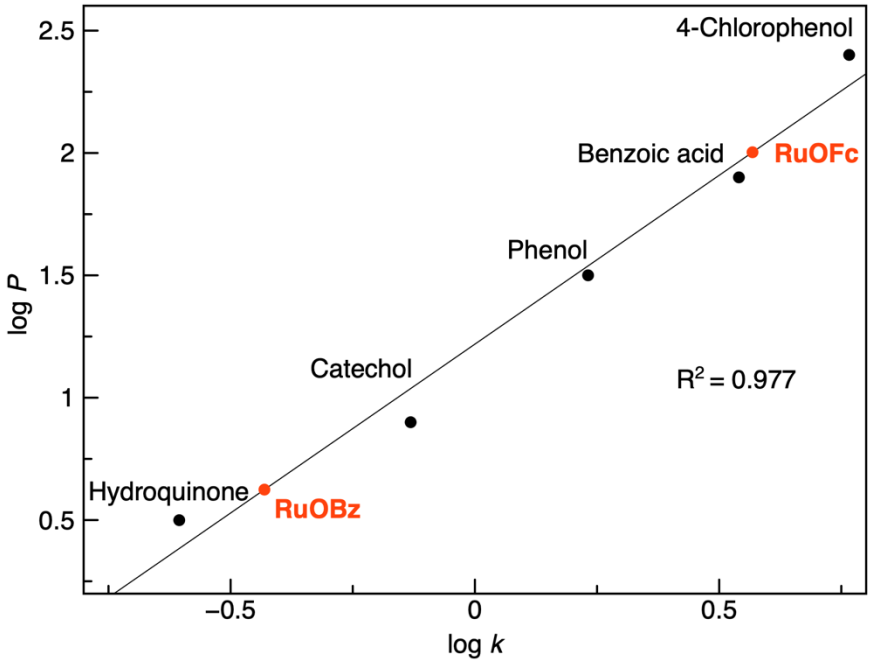

Fig. S10 log *P* vs log *k* calibration curve based on the 5 standard compounds (black points). Orange points show the extrapolated log *P* values of **RuOBz** and **RuOFc**.

3. Aquation Kinetics Studies

Solutions of **RuOFc** and **RuOBz** were prepared at concentrations of 160 µM in aqueous solutions of 16 mM of 3-(*N*-morpholino)propanesulfonic acid (MOPS) buffer at pH 7.4. Changes in the electronic absorption spectra were monitored over time at 37 °C until no further spectral changes were observed. The absorbance at wavelengths of the most significant spectral changes was plotted as a function of time and fitted into a first-order exponential model to obtain the half-lives of the compounds in aqueous solution. Results are reported as the average of three independent replicates ± standard deviation (SD).

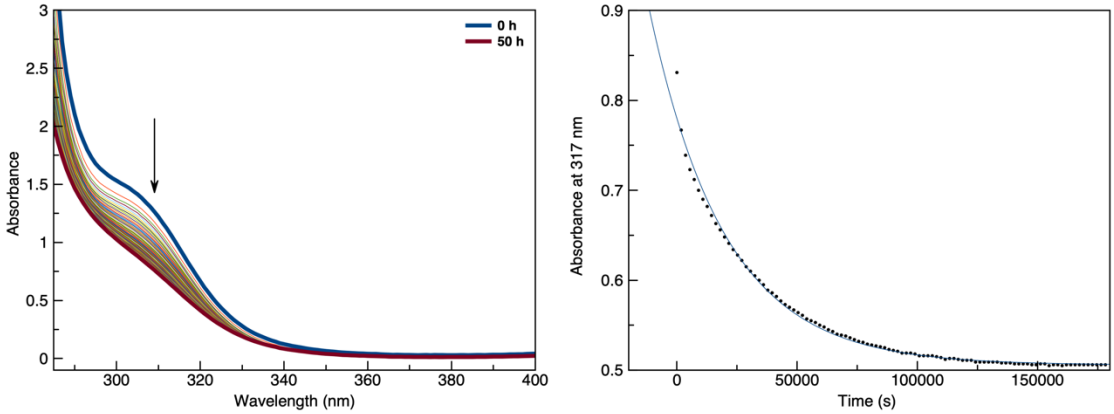

Fig. S11 Left: evolution of the UV-vis spectrum of **RuOBz** (160 µM) in pH 7.4 MOPS-buffered (16 mM) aqueous solution over a 50 h period at 37 °C. Right: plot of absorbance at 317 nm versus time with the best exponential fit.

4. Electrochemical Studies

Cyclic Voltammetry. Electrochemical measurements were carried out using a Pine WaveNow potentiostat with a three-electrode setup consisting of a glassy carbon working electrode, a platinum counter electrode, and a Ag wire quasi-reference electrode. Complexes were dissolved in anhydrous DMF with 0.10 M $[Bu_4N][PF_6]$ (TBAP) as the supporting electrolyte. Potentials were referenced using an internal standard of either the ferrocene/ferricenium couple at 0.45 V or the cobaltocene/cobaltocenium couple at –0.76 V vs the standard calomel electrode (SCE).

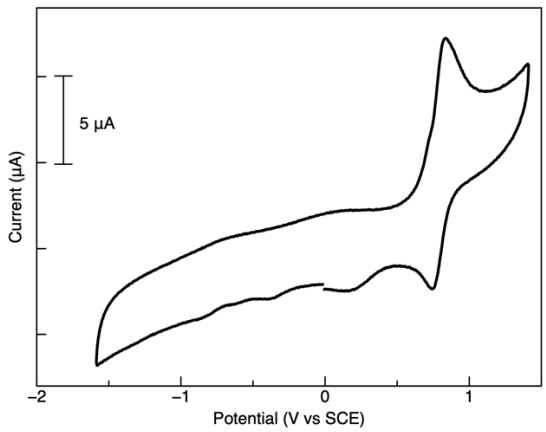

Fig. S12 Cyclic voltammogram of ferrocenecarboxylic acid in DMF with 0.1 M $[Bu_4N][PF_6]$ (TBAP) at 25 °C and 0.1 V/s scan rate.

5. Computational Studies

DFT calculations were performed using Gaussian 16.[9] All calculations were carried out using the hybrid B3LYP functional[10,11]. The LANL2DZ basis set and effective core potential[12] were utilized for both ruthenium and iron atoms, and the 6-31G(d,p) basis set[13,14] was used for the other elements. A quadratically convergent self-consistent field (QC-SCF)[15] procedure was used. Geometry optimizations were performed in the gas phase without symmetry restraints. The crystal structures of **Ru265′**,[16] **RuOBz**, and **RuOFc** were used as the starting geometries of the optimization. After geometry optimization, frequency calculations were carried out to ensure that the geometries had converged to local minima on the potential energy surface. The Cartesian coordinates of all optimized structures are provided as part of the Electronic Supplementary Information. Using these optimized geometries, subsequent molecular orbital calculations were performed using a polarizable continuum model (PCM)[17] to simulate solvation of the compounds in water. The isodensity surface plots of the frontier molecular orbitals are rendered at an isovalue of 0.02 using Avogadro 1.2.0.[18]

6. Cellular Studies

Cell Lines and Culture Conditions. HeLa and HEK293T cell lines were obtained from American Type Culture Collection (ATCC) and cultured as adherent monolayers in Dulbecco's Modified Eagle's Medium (DMEM) supplemented with 10% fetal bovine serum (FBS). All cell lines were grown in a humidified incubator at 37 °C with an atmosphere of 5% CO_2. Cells were passed at 80−90% confluence using trypsin/ethylenediaminetetraacetic acid (EDTA). Cells were tested for mycoplasma contamination through the commercial service provided by the College of Veterinary Medicine at Cornell University.

Cytotoxicity Assay. HEK293T or HeLa cells were seeded in 96-well plates with 4000 cells/well in 100 μL of growth media and allowed to reattach overnight. The following day, the culture media was removed and replaced with 200 μL of media containing varying concentration of the complexes. The plates were then incubated for 48 h, the medium was removed from the wells, and 3-(4,5-dimethylthiazol-2-yl)-2,5-tetrazolium bromide (MTT) in DMEM (200 μL, 1 mg/mL) was added. The additional 48 h incubation was performed to ensure that the cells were in the logarithmic growth phase and that the cells had adequate time to regrow after exposure to the complexes. After 4 h, the media was removed, and the purple formazan crystals were dissolved in 200 μL of an 8:1 mixture of DMSO and pH 10 glycine buffer. The absorbance at 570 nm in each well was then measured. Cell viability was determined by normalizing the absorbance of the treated wells to untreated wells. Results are reported as the average cell viability of six replicates per concentration from three independent trials.

Cellular Uptake Assay. HEK293T or HeLa cells were grown to near confluence in 6-well plates. On the day of the experiment, the culture media was removed, and the cells were treated with fresh media containing 0 or 50 μM complex and incubated for 2 h at 37 ºC. The culture media was then removed, and the adherent cells were washed with 3 × 1 mL of PBS and harvested with trypsin before being pelleted by centrifugation. The cell pellet was suspended in 300 μL of pH 7.4 lysis buffer containing 1% w/v 3-[3-cholamidopropyl)dimethylammonio]-1-propanesulfonate (CHAPS), 5 mM EDTA, 50 mM tris(hydroxymethyl)aminomethane (Tris) and 100 mM NaCl. The suspension was vortexed for 30 s and incubated on ice for 45 min. The cell lysate was centrifuged to remove pelleted debris, and the supernatant was transferred to a

clean tube prior to analysis. The Ru content of the lysate was determined using GFAAS and was normalized to the protein content of the sample, which was determined using the bicinchoninic acid (BCA) assay kit following manufacturer instructions (ThermoFisher). Results are reported as the average mass ratio of Ru to protein (pg/μg) in each sample ± SD (n = 4–6).

Mitochondrial Ca^{2+} Uptake in Permeabilized Cells. HEK293T cells were grown to near confluency in a T25 flask and harvested using trypsin/EDTA. The cells were pelleted by centrifugation and suspended in cold PBS supplemented with 5 mM EDTA (pH 7.4) and counted using trypan blue. The remaining cells were pelleted by centrifugation at 600 × g for 5 min and resuspended in ice cold high KCl solution (125 mM KCl, 20 mM 4-(2-hydroxyethyl)-1-piperazineethanesulfonic acid (HEPES), 2 mM K_2HPO_4, 5 mM glutamate, 5 mM malate, 1 mM $MgCl_2$, pH 7.2 with KOH) supplemented with 80 μM digitonin and 1 μM thapsigargin. The cells were incubated on ice for 25 min and centrifuged at 220 × g for 10 min at 4 °C. The pelleted cells were then resuspended in high KCl solution containing 1 μM Calcium Green 5N and 2 mM sodium succinate to a final density of 5×10^6 cells/mL. For each experiment, 100 μL of the cell suspension was placed in each well of a black-walled 96 well plate, treated with the desired concentration of the test complex. The fluorescence measurement was then performed at 37 °C. The background fluorescence of each well was recorded for at least 45 s prior to addition of 10 μM $CaCl_2$. The change in fluorescence of the dye (ex. 488 / em. 528) in response to Ca^{2+} was recorded every 5 s for at least 120 s or until the fluorescence returned to the baseline. The *m*Ca^{2+} uptake rate was calculated as the slope of the linear fit of the first 25 s of the fluorescence response. The Ca^{2+} uptake rate of treated cells was normalized to that of the controls cells (0% inhibition). Data are presented as the average of three independent replicates ± SD.

Mitochondrial Membrane Potential Assay. HeLa cells (1×10^5) were seeded in 35 mm glass-bottomed dishes and incubated overnight at 37 °C. On the next day, cells were treated with the desired compound (50 μM) and incubated for a further 24 h. The culture media was removed and replaced with fresh media containing 10 μM JC-1 dye and incubated at 37 °C in the dark for 30 min. The media was removed, and the cells were washed with 2 × 1 mL PBS, and 1 mL extracellular medium (ECM; 135 mM NaCl, 20 mM HEPES, 5 mM KCl, 1 mM $MgCl_2$, 1 mM $CaCl_2$) was added. For the positive control dishes, cells were treated with 50 μM carbonyl cyanide *m*-chlorophenyl hydrazine (CCCP) in ECM, and the cells were imaged without the removal of CCCP. The cells were imaged using a EVOS M5000 microscope (Thermofisher, USA). The JC-1 monomers were visualized using a 482/25 nm LED light excitation and a 524/24 nm green emission filter, whereas the J-aggregates were visualized using a 585/29 nm LED light excitation and a 628/32 nm red emission filter. The cellular images were analyzed using ImageJ, and the average red/green ratio of the corrected total cellular fluorescence (CTCF) was determined using at least 8 independent cells and was normalized to untreated control cells ($[red/green]_{control} = 1$).

Mitochondrial Ca^{2+} Uptake in Intact HeLa Cells Using Rhod2AM. HeLa cells (5×10^4) were seeded in an 8-well μ-slide (Ibidi USA, Inc., Fitchburg, WI) and incubated overnight at 37 °C. The following day, cells were treated with the desired metal complex (50 μM) in DMEM supplemented with 10% FBS for 3.5 h at 37 °C. The culture media was removed, and the cells were washed with PBS before the incubation in ECM supplemented with 10 mM glucose, 3.2 mg/mL bovine serum albumin (BSA), 0.003% Pluronic F127, and 2 μM Rhod2AM (Molecular Probes) in the dark for 30 min at room temperature. The solution was then removed, and the cells were washed with ECM before incubated for an additional 30 min in the dark at room

temperature with fresh ECM supplemented with 10 mM glucose and 3.2 mg/mL BSA. The buffer was then removed, and the cells were washed with ECM and treated with ECM supplemented with 10 mM glucose and 3.2 mg/mL BSA. The cells were incubated for 15 min at 37 °C before imaging using a Zeiss LSM 710 confocal laser-scanning microscope with an excitation of 561 nm and an emission window of 568–712 nm. After ~ 30 s of baseline recording, histamine (100 µM) was added to the dish and fluorescence images were collected every 3 s to monitor *m*Ca^{2+} uptake. The cellular images were analyzed using ImageJ, and the CTCF was determined using at least 6 cells. Results are reported as the average of at least three independent replicates ± SD.

Table S3 Cellular uptake of Ru265, **RuOBz**, and **RuOFc** in HeLa cells after 2 h incubation.

	Ru265	**RuOBz**	**RuOFc**
(pg Ru / µg protein)	44 ± 12	63 ± 26	343 ± 79

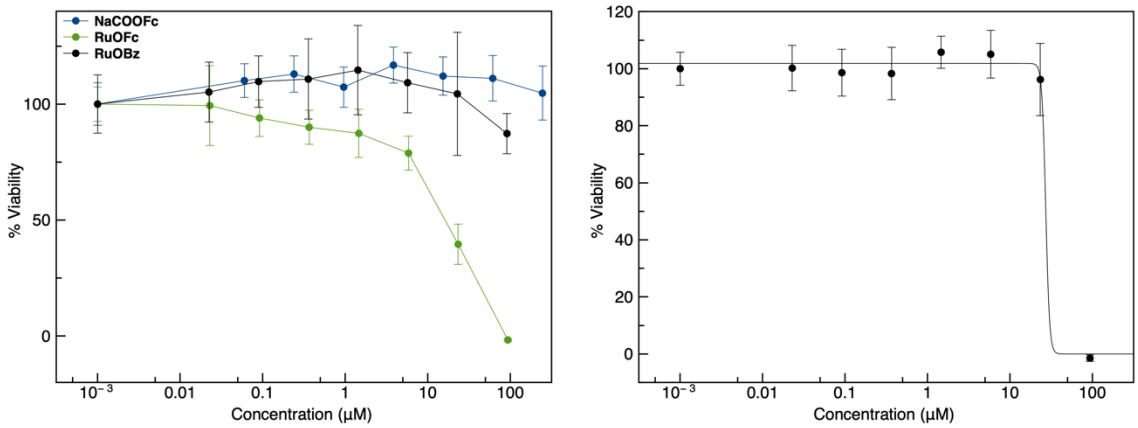

Fig. S13 Left: cytotoxicity dose-response curves of **RuOBz**, **RuOFc**, and sodium ferrocenecarboxylates (NaCOOFc) in HEK293T cells. Right: cytotoxicity dose-response curve of **RuOFc** in HeLa cells.

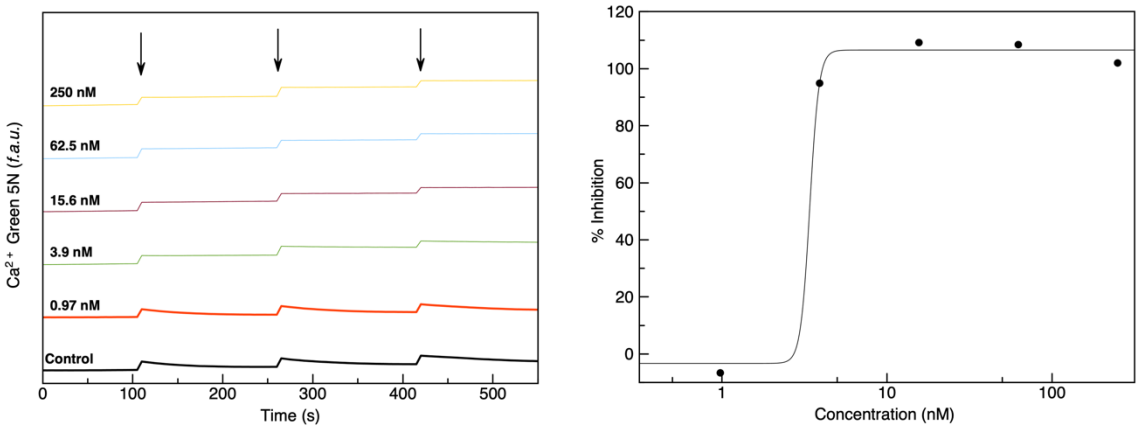

Fig. S14 Left: traces of extramitochondrial Ca^{2+} clearance after addition of 10 µM Ca^{2+} in permeabilized HEK293T cells treated with varying concentration of Ru265. The arrows indicate the time of Ca^{2+} addition. Right: dose-response curve of *m*Ca^{2+} uptake inhibition by Ru265.

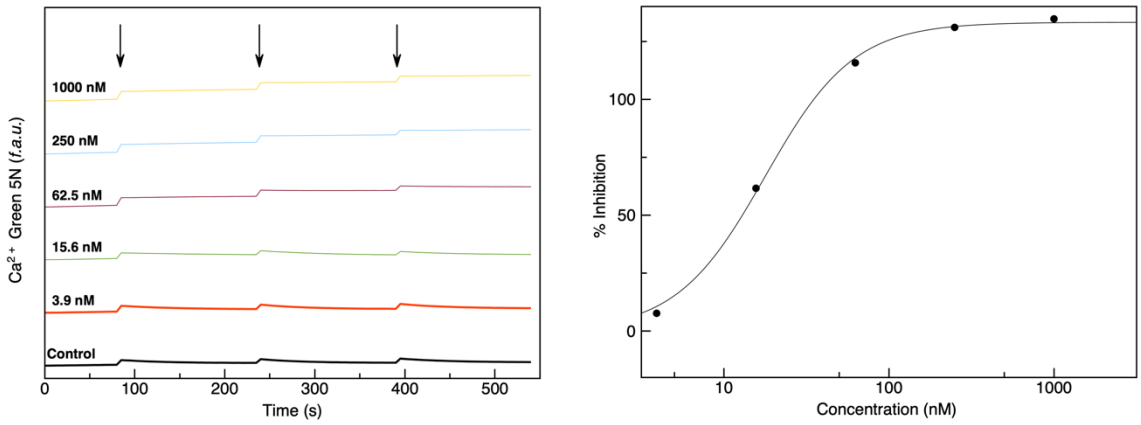

Fig. S15 Left: traces of extramitochondrial Ca^{2+} clearance after addition of 10 µM Ca^{2+} in permeabilized HEK293T cells treated with varying concentration of **RuOBz**. The arrows indicate the time of Ca^{2+} addition. Right: dose-response curve of *m*Ca^{2+} uptake inhibition by **RuOBz**.

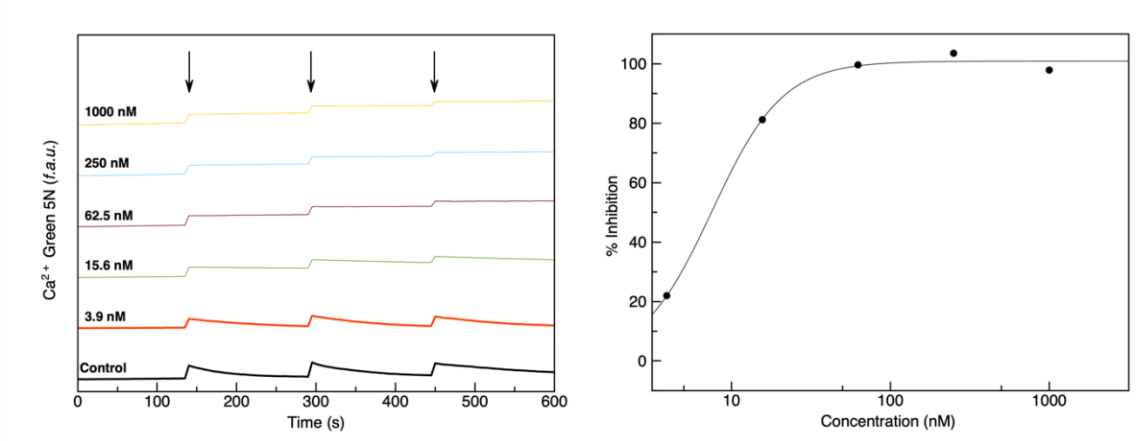

Fig. S16 Left: traces of extramitochondrial Ca^{2+} clearance after addition of 10 µM Ca^{2+} in permeabilized HEK293T cells treated with varying concentration of **RuOFc**. The arrows indicate the time of Ca^{2+} addition. Right: dose-response curve of *m*Ca^{2+} uptake inhibition by **RuOFc**.

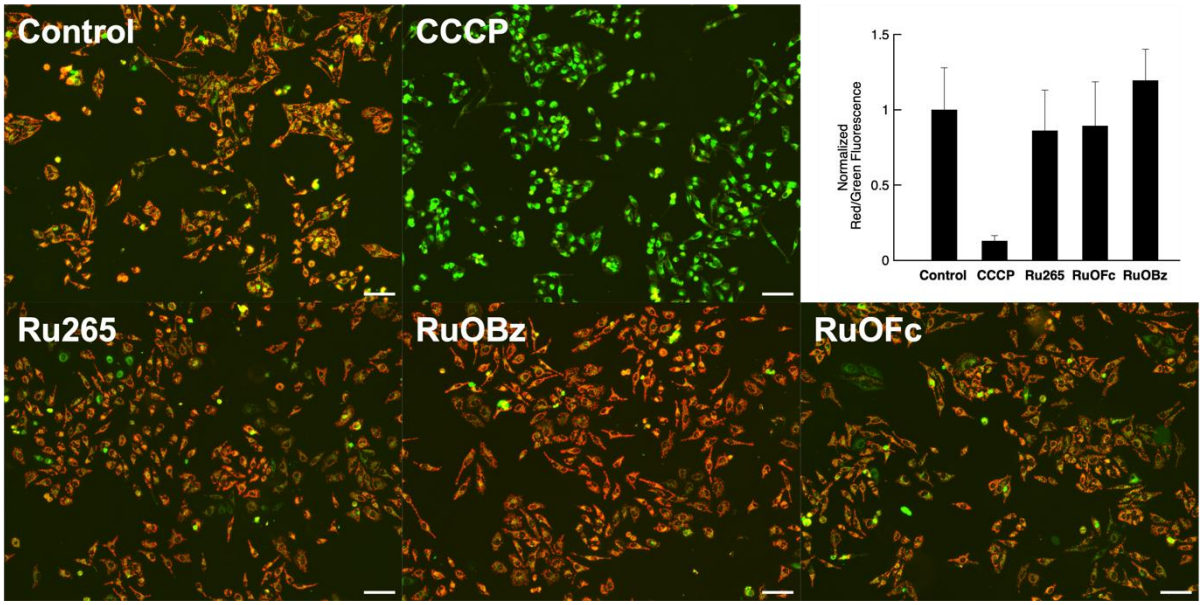

Fig. S17 Fluorescent microscopy images of HeLa cells treated with JC-1 dye and 50 µM of CCCP, Ru265, **RuOBz**, and **RuOFc** (Scale bar = 100 µm). Top right: normalized red/green fluorescence intensity of all images.

7. References

1 J. J. Woods, N. Nemani, S. Shanmughapriya, A. Kumar, M. Zhang, S. R. Nathan, M. Thomas, E. Carvalho, K. Ramachandran, S. Srikantan, P. B. Stathopulos, J. J. Wilson and M. Madesh, A Selective and Cell-Permeable Mitochondrial Calcium Uniporter (MCU) Inhibitor Preserves Mitochondrial Bioenergetics after Hypoxia/Reoxygenation Injury, *ACS Cent. Sci.*, 2019, **5**, 153–166.

2 A. F. Neto, J. Miller, V. F. de Andrade, S. Y. Fujimoto, M. M. de Freitas Afonso, F. C. Archanjo, V. A. Darin, M. L. Andrade e Silva, Á. D. L. Borges and G. Del Ponte, New Synthesis of Ferrocene Monocarboxylic Acid and Systematic Studies on the Preparation of Related Key-Intermediates, *Z. Anorg. Allg. Chem.*, 2002, **628**, 209–216.

3 G. M. Sheldrick, SHELXT – Integrated Space-Group and Crystal-Structure Determination, *Acta Crystallogr. Sect. A Found. Adv.*, 2015, **71**, 3–8.

4 G. M. Sheldrick, A Short History of SHELX, *Acta Crystallogr. Sect. A Found. Crystallogr.*, 2008, **64**, 112–122.

5 P. Müller, Practical Suggestions for Better Crystal Structures, *Crystallogr. Rev.*, 2009, **15**, 57–83.

6 O. V. Dolomanov, L. J. Bourhis, R. J. Gildea, J. A. K. Howard and H. Puschmann, OLEX2: A Complete Structure Solution, Refinement and Analysis Program, *J. Appl. Crystallogr.*, 2009, **42**, 339–341.

7 OECD, Test No. 117: Partition Coefficient (n-octanol/water), HPLC Method, https://www.oecd-ilibrary.org/environment/test-no-117-partition-coefficient-n-octanol-water-hplc-method_9789264069824-en, (accessed November 2022).

8 S. Tshepelevitsh, K. Hernits, J. Jenčo, J. M. Hawkins, K. Muteki, P. Solich and I. Leito, Systematic Optimization of Liquid-Liquid Extraction for Isolation of Unidentified Components, *ACS Omega*, 2017, **2**, 7772–7776.

9 M. J. Frisch, G. W. Trucks, H. B. Schlegel, G. E. Scuseria, M. A. Robb, J. R. Cheeseman, G. Scalmani, V. Barone, G. A. Petersson, H. Nakatsuji, X. Li, M. Caricato, A. V. Marenich, J. Bloino, B. G. Janesko, R. Gomperts, B. Mennucci, H. P. Hratchian, J. V.

Ortiz, A. F. Izmaylov, J. L. Sonnenberg, D. Williams-Young, F. Ding, F. Lipparini, F. Egidi, J. Goings, B. Peng, A. Petrone, T. Henderson, D. Ranasinghe, V. G. Zakrzewski, J. Gao, N. Rega, G. Zheng, W. Liang, M. Hada, M. Ehara, K. Toyota, R. Fukuda, J. Hasegawa, M. Ishida, T. Nakajima, Y. Honda, O. Kitao, H. Nakai, T. Vreven, K. Throssell, J. A. M. Jr., J. E. Peralta, F. Ogliaro, M. J. Bearpark, J. J. Heyd, E. N. Brothers, K. N. Kudin, V. N. Staroverov, T. A. Keith, R. Kobayashi, J. Normand, K. Raghavachari, A. P. Rendell, J. C. Burant, S. S. Iyengar, J. Tomasi, M. Cossi, J. M. Millam, M. Klene, C. Adamo, R. Cammi, J. W. Ochterski, R. L. Martin, K. Morokuma, O. Farkas, J. B. Foresman and D. J. Fox, *Gaussian 16, Revision C.01*, Gaussian, Inc., Wallingford, CT, 2016.

10 C. Lee, W. Yang and R. G. Parr, Development of the Colle-Salvetti Correlation-Energy Formula into a Functional of the Electron Density, *Phys. Rev. B*, 1988, **37**, 785–789.

11 A. D. Becke, Density-functional Thermochemistry. III. The Role of Exact Exchange, *J. Chem. Phys.*, 1993, **98**, 5648–5652.

12 P. J. Hay and W. R. Wadt, Ab Initio Effective Core Potentials for Molecular Calculations. Potentials for K to Au Including the Outermost Core Orbitals, *J. Chem. Phys.*, 1985, **82**, 299–310.

13 W. J. Hehre, R. Ditchfield and J. A. Pople, Self-Consistent Molecular Orbital Methods. XII. Further Extensions of Gaussian-Type Basis Sets for Use in Molecular Orbital Studies of Organic Molecules, *J. Chem. Phys.*, 1972, **56**, 2257–2261.

14 P. C. Hariharan and J. A. Pople, The Influence of Polarization Functions on Molecular Orbital Hydrogenation Energies, *Theor. Chim. Acta*, 1973, **28**, 213–222.

15 G. B. Bacskay, A Quadratically Convergent Hartree-Fock (QC-SCF) Method. Application to Closed Shell Systems, *Chem. Phys.*, 1981, **61**, 385–404.

16 J. J. Woods, J. Lovett, B. Lai, H. H. Harris and J. J. Wilson, Redox Stability Controls the Cellular Uptake and Activity of Ruthenium-Based Inhibitors of the Mitochondrial Calcium Uniporter (MCU), *Angew. Chem. Int. Ed.*, 2020, **59**, 6482–6491.

17 S. Miertuš, E. Scrocco and J. Tomasi, Electrostatic Interaction of a Solute with a Continuum. A Direct Utilizaion of AB Initio Molecular Potentials for the Prevision of Solvent Effects, *Chem. Phys.*, 1981, **55**, 117–129.

18 M. D. Hanwell, D. E. Curtis, D. C. Lonie, T. Vandermeersch, E. Zurek and G. R. Hutchison, Avogadro: An Advanced Semantic Chemical Editor, Visualization, and Analysis Platform, *J. Cheminf.*, 2012, **4**, 17.